

Supporting Information

Layered cobalt hydrotalcite as an advanced lithium-ion anode material with high capacity and rate capability

Long Pan, Haijian Huang, Markus Niederberger*

*Laboratory for Multifunctional Materials, Department of Materials, ETH Zurich, Vladimir-Prelog-
Weg 5, 8093, Zurich, Switzerland*

** E-mail: long.pan@mat.ethz.ch*

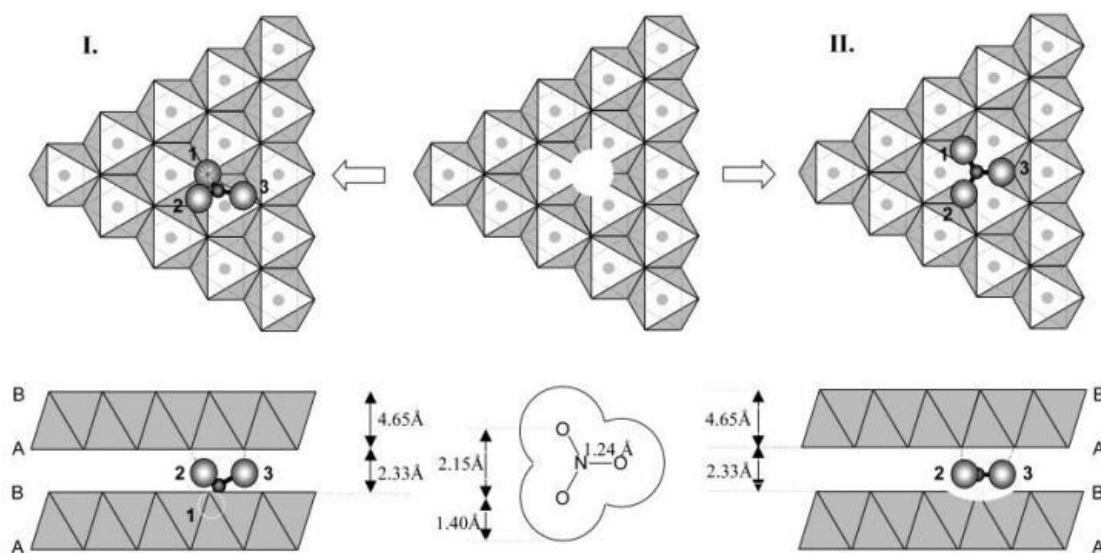


Figure S1. Configurations of NO_3^- anions in the interlayer gallery of LCH. At the $-\text{OH}$ vacancy sites, the NO_3^- anions have two configurations: (1) The NO_3^- anions could be integrated into the brucite-like plane *via* one of its three O atoms (model I); (2) The NO_3^- anions are also possible to attach to the $-\text{OH}$ vacancies with a D_{3h} site symmetry, as illustrated in model II. Adapted with permission.^[S1]

Copyright 2003 American Chemical Society.

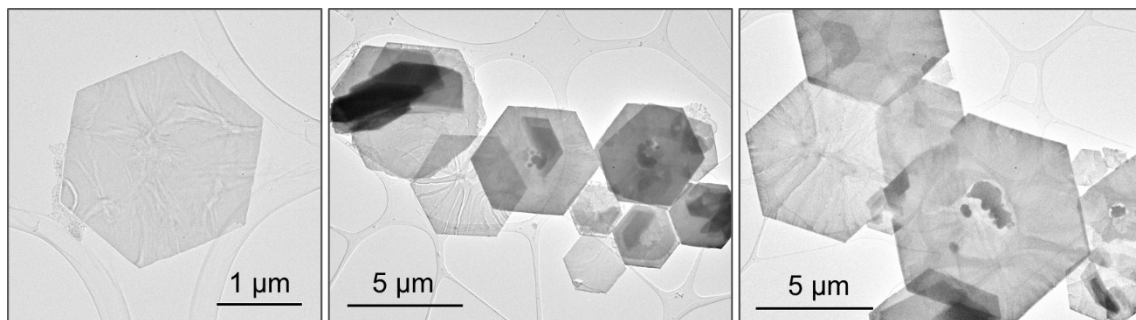


Figure S2. TEM images of the LCH nanosheets.

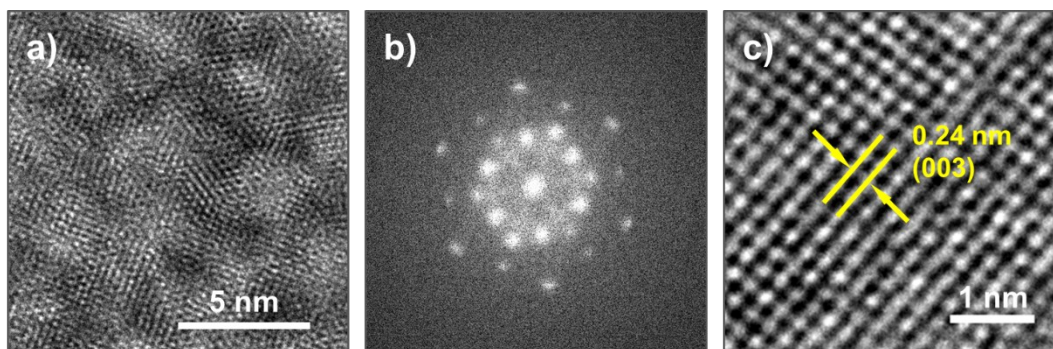


Figure S3. (a) HRTEM image and (b) corresponding fast Fourier transform (FFT) pattern, and (c) HRTEM image of the LCH nanosheets.

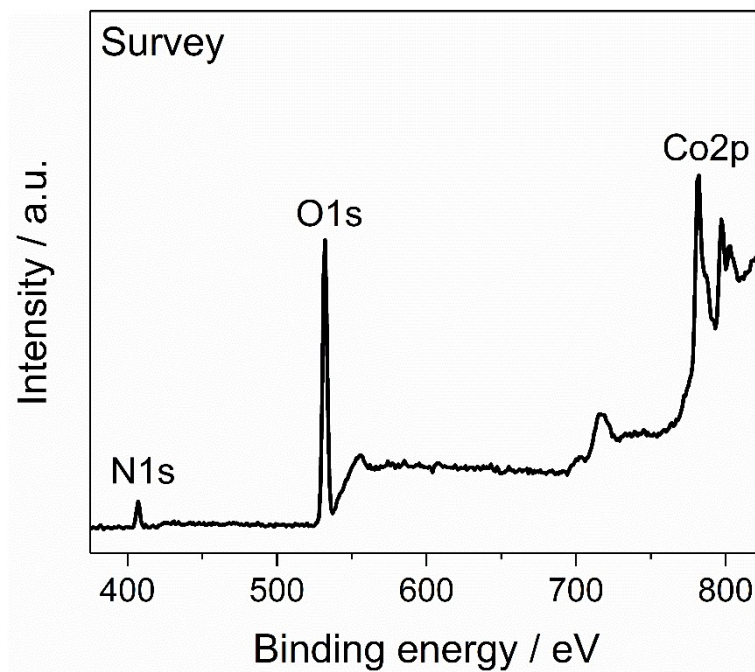


Figure S4. XPS survey spectrum of the LCH nanosheets.

Table S1. Atomic ratio (at%) of Co, O, and N in the LCH nanosheets obtained from XPS analysis.

	Co	O	N
Theoretical ratio	22.2	66.7	11.1
Experimental ratio	22.9	66.6	10.5

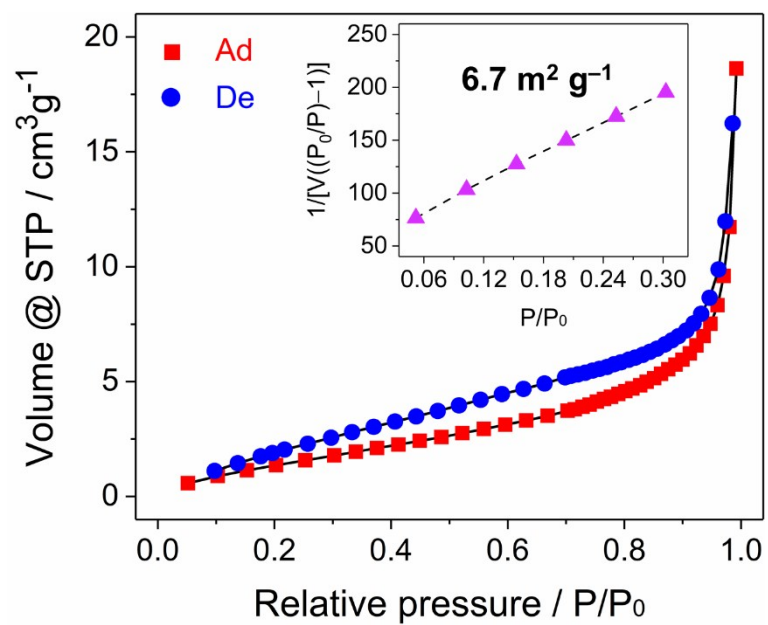


Figure S5. N₂ adsorption-desorption isotherms and BET surface area (inset) of the LCH nanosheets.

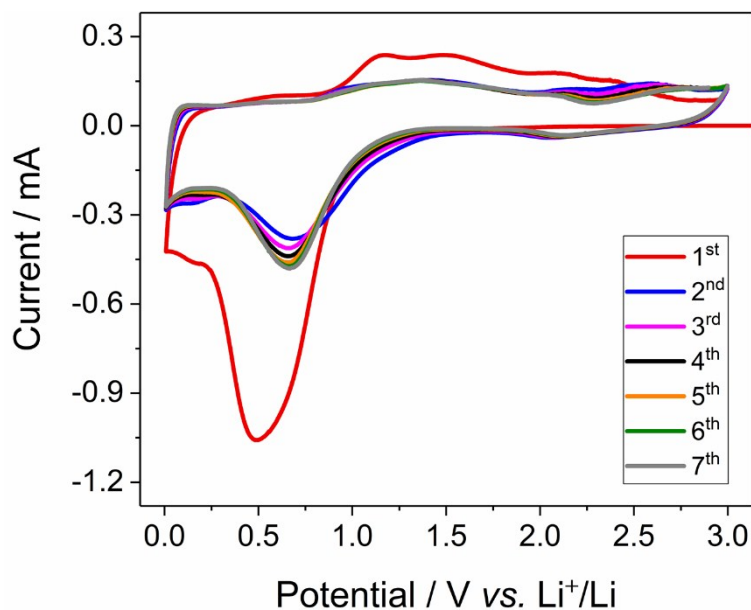


Figure S6. The first seven CV curves of the LCH nanosheets. Note that a significant difference between the first CV curve and the others is witnessed in the cathodic process within the voltage range of around 0.9–0.01 V. This difference is mainly attributed to the formation of solid-electrolyte interphase (SEI) layer, which consumes electrolyte and causes irreversible capacity loss. This capacity loss is also observed in the discharging/charging profiles (**Figure 2a** and **2b**). After forming a stable SEI layer, the Li^+ storage became stable and reversible, therefore the CV curves from 2nd cycle were almost unchanged. The pair of small, broad peaks at around 2.0 V might be assigned to the Li^+ intercalation into the LCH. In the cathodic scans, the peak at ca. 0.7 V was attributed to the conversion reaction of LCH with Li^+ ($\text{LCH} + x\text{Li}^+ + xe^- \rightarrow \text{Co}$), which was also verified by the discharging/charging profiles (**Figure 2b**). In the anodic scans, the multiple peaks at the voltage range of 1.2–1.6 V corresponded to the Li^+ extraction from LCH.

Table S2. Comparison of cyclability of LCH with other conversion-type anode materials.

Electrode materials	Specific current mA g ⁻¹	Cycle number	Specific capacity mA h g ⁻¹	Mass loading mg cm ⁻²	Electrode composition ^a	Ref.
Co(OH) ₂ /rGO	200	30	950	1.5–2.0	75 : 15 : 10	[S2]
Co(OH) ₂ /Co ₃ O ₄	58	40	1100	1.0–1.5	80: 10 : 10	[S3]
Co ₃ O ₄ /MWCNT	100	100	813	–	70: 20 : 10	[S4]
Co ₃ O ₄ /TiO ₂	200	100	803	–	70: 20 : 10	[S5]
	100	350	400			
Co ₃ O ₄ /CNT	100	100	700	–	85: 10 : 5	[S6]
Co ₃ O ₄ /N-Carbon	500	300	795	1.37	80: 10 : 10	[S7]
Fe ₃ O ₄ /carbon	1000	400	581	0.62–0.78	60: 20 : 20	[S8]
Fe ₃ O ₄ /carbon	1000	300	746	0.32	80: 10 : 10	[S9]
Fe ₃ O ₄ /rGO	50	50	1048.5	–	80: 10 : 10	[S10]
Fe ₃ O ₄ /carbon	500	350	833.5	–	70: 20 : 10	[S11]
LCH	500	600	743.9	1.0	60 : 30 :10	This work
	2000	2000	643.4			

a. Electrode composition means the weight ratio of active materials : carbon black : binder.

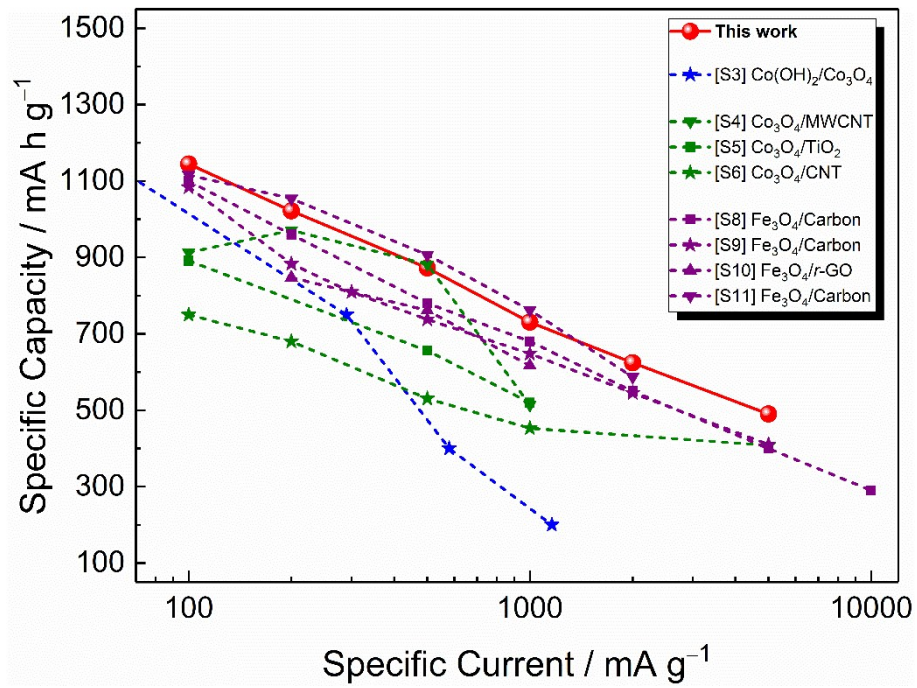


Figure S7. Comparison of rate capabilities of LCH with other conversion-type anode materials.

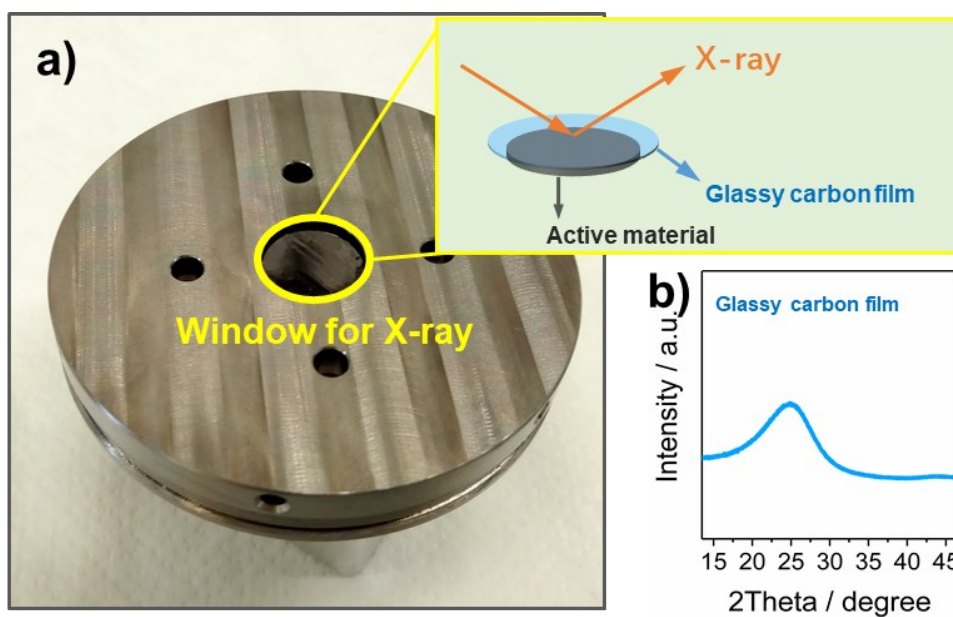


Figure S8. (a) Photograph and schematic illustration (inset) of the device for *operando* XRD measurements, and (b) XRD pattern of the glassy carbon foil.

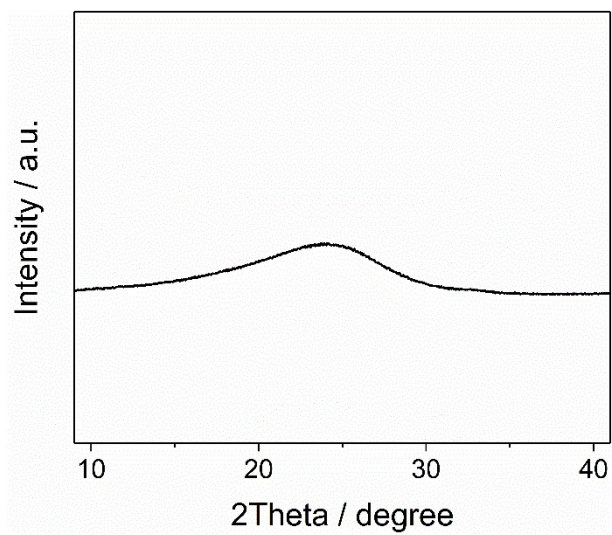


Figure S9. XRD pattern of LCH after charging to 3.0 V at 50 mA g⁻¹. The broad peak is attributed to the glassy carbon foil (**Figure S8**).

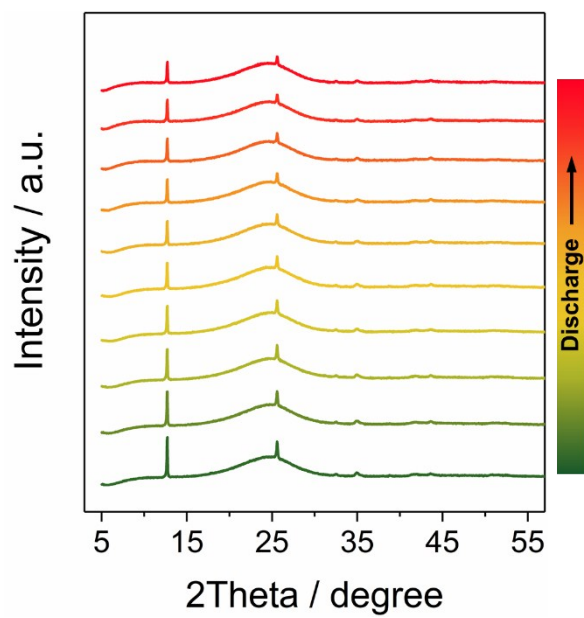


Figure S10. *Operando* XRD patterns of the LCH nanosheets during the first discharge at 200 mA g^{-1} .

It can be observed that the intensities of (00 l) peaks keep decreasing during the Li^+ insertion.

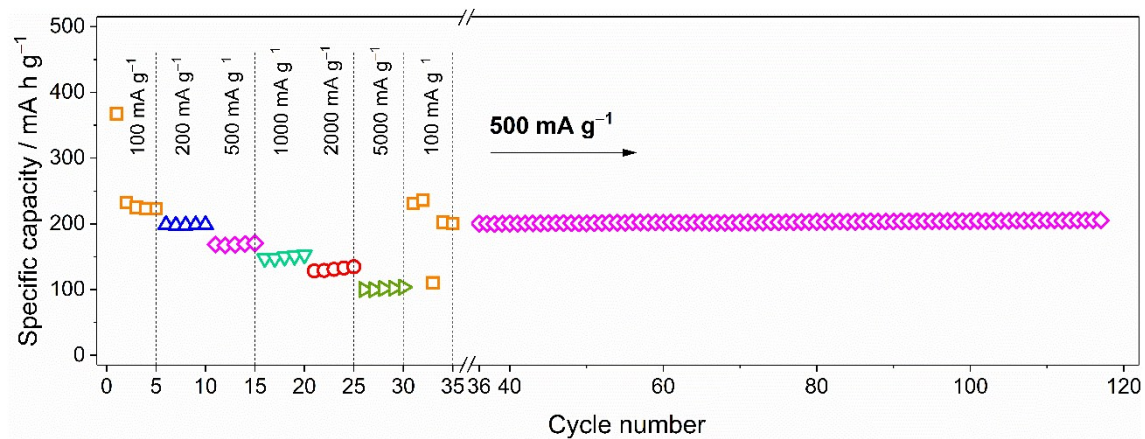


Figure S11. The rate capability and cycling performance (specific current = 500 mA g^{-1}) of carbon black. The mass loading of carbon black is around 1 mg cm^{-2} . The reversible capacity of carbon black at 500 mA g^{-1} is *ca.* 200 mA h g^{-1} , which contributes $\sim 60 \text{ mA h g}^{-1}$ to the total capacity ($743.9 \text{ mA h g}^{-1}$) of LCH, indicating that the capacity contribution ($\approx 8\%$) of carbon black is small.

References

- [S1] R. Xu, H. C. Zeng, *Chem. Mater.* **2003**, *15*, 2040.
- [S2] Y.-S. He, D.-W. Bai, X. Yang, J. Chen, X.-Z. Liao, Z.-F. Ma, *Electrochem. Commun.* **2010**, *12*, 570.
- [S3] X.-l. Huang, X. Zhao, Z.-l. Wang, L.-m. Wang, X.-b. Zhang, *J. Mater. Chem.* **2012**, *22*, 3764.
- [S4] G. Huang, F. F. Zhang, X. C. Du, Y. L. Qin, D. M. Yin, L. M. Wang, *ACS Nano* **2015**, *9*, 1592.
- [S5] H. B. Geng, H. X. Ang, X. G. Ding, H. T. Tan, G. L. Guo, G. L. Qu, Y. G. Yang, J. W. Zheng, Q. Y. Yan, H. W. Gu, *Nanoscale* **2016**, *8*, 2967.
- [S6] D. Gu, W. Li, F. Wang, H. Bongard, B. Spliethoff, W. Schmidt, C. Weidenthaler, Y. Y. Xia, D. Y. Zhao, F. Schüth, *Angew. Chem., Int. Ed.* **2015**, *54*, 7060.
- [S7] Y. Sun, F. Z. Huang, S. K. Li, Y. H. Shen, A. J. Xie, *Nano Res.* **2017**, *10*, 3457.
- [S8] J. Mao, D. Niu, N. Zheng, G. Jiang, W. Zhao, J. Shi, Y. Li, *ACS Sustainable Chem. Eng.* **2019**, *7*, 3424.
- [S9] W. Han, X. Qin, J. Wu, Q. Li, M. Liu, Y. Xia, H. Du, B. Li, F. Kang, *Nano Res.* **2018**, *11*, 892.
- [S10] Y.-J. Duan, D.-L. Zhao, X.-H. Liu, H.-X. Yang, W.-J. Meng, M. Zhao, X.-M. Tian, X.-Y. Han, *J. Alloys Compd.* **2019**, *779*, 466.
- [S11] C. Han, L. Xu, H. Li, R. Shi, T. Zhang, J. Li, C.-P. Wong, F. Kang, Z. Lin, B. Li, *Carbon*, **2018**, *140*, 296.